AD_____

MIPR NUMBER 96MM6730

TITLE: Portable Oxygen Generation for Medical Applications

PRINCIPAL INVESTIGATOR: Timothy R. Armstrong, Ph.D.

CONTRACTING ORGANIZATION: Department of Energy
Richland, WA 99352

REPORT DATE: July 1997

TYPE OF REPORT: Final

PREPARED FOR: Commander
U.S. Army Medical Research and Materiel Command
Fort Detrick, Frederick, Maryland 21702-5012

REPORT DOCUMENTATION PAGE

Form Approved
OMB No. 0704-0188

1. AGENCY USE ONLY *(Leave blank)*	2. REPORT DATE	3. REPORT TYPE AND DATES COVERED
	July 1997	Final (8 May 96 - 1 Jul 97)

4. TITLE AND SUBTITLE
Portable Oxygen Generation for Medical Applications

5. FUNDING NUMBERS
96MM6730

6. AUTHOR(S)
Timothy R. Armstrong, Ph.D.

7. PERFORMING ORGANIZATION NAME(S) AND ADDRESS(ES)
Department of Energy
Richland, Washington 99352

8. PERFORMING ORGANIZATION REPORT NUMBER

9. SPONSORING/MONITORING AGENCY NAME(S) AND ADDRESS(ES)
Commander
U.S. Army Medical Research and Materiel Command
Fort Detrick, Frederick, Maryland 21702-5012

10. SPONSORING/MONITORING AGENCY REPORT NUMBER

11. SUPPLEMENTARY NOTES

12a. DISTRIBUTION / AVAILABILITY STATEMENT
Approved for public release; distribution unlimited

12b. DISTRIBUTION CODE

13. ABSTRACT *(Maximum 200*

A prototypical high-temperature planar oxygen generator was developed within one year. This generator utilizes yttria stabilized zirconia electrolyte and dope lanthanum manganite as the electrodes and separator plate. Several stack (1 to 3-cell) were constructed and tested. The tests demonstrated that: 1) all 25 cm^2 of the active area was operational, 2) the cells possessed a low area specific resistance that improved with time, and 3) stack power consumption decreased with time without affecting oxygen output. Important accomplishments were achieved in the areas of separator plate fabrication, metallic seal development, and stack assembly and testing.

14. SUBJECT TERMS	15. NUMBER OF PAGES
oxygen generator, yttria stabilized zirconia	44
	16. PRICE CODE

17. SECURITY CLASSIFICATION OF REPORT	18. SECURITY CLASSIFICATION OF THIS PAGE	19. SECURITY CLASSIFICATION OF ABSTRACT	20. LIMITATION OF ABSTRACT
Unclassified	Unclassified	Unclassified	Unlimited

FOREWORD

Opinions, interpretations, conclusions and recommendations are those of the author and are not necessarily endorsed by the U.S. Army.

____ Where copyrighted material is quoted, permission has been obtained to use such material.

____ Where material from documents designated for limited distribution is quoted, permission has been obtained to use the material.

TRA Citations of commercial organizations and trade names in this report do not constitute an official Department of Army endorsement or approval of the products or services of these organizations.

____ In conducting research using animals, the investigator(s) adhered to the "Guide for the Care and Use of Laboratory Animals," prepared by the Committee on Care and Use of Laboratory Animals of the Institute of Laboratory Resources, National Research Council (NIH Publication No. 86-23, Revised 1985).

____ For the protection of human subjects, the investigator(s) adhered to policies of applicable Federal Law 45 CFR 46.

____ In conducting research utilizing recombinant DNA technology, the investigator(s) adhered to current guidelines promulgated by the National Institutes of Health.

____ In the conduct of research utilizing recombinant DNA, the investigator(s) adhered to the NIH Guidelines for Research Involving Recombinant DNA Molecules.

____ In the conduct of research involving hazardous organisms, the investigator(s) adhered to the CDC-NIH Guide for Biosafety in Microbiological and Biomedical Laboratories.

Timothy R Aubrey 7-21-97

PI - Signature Date

Table of Contents

1. Introduction

The production of oxygen is of vital interest in many applications, from space missions to supplying air to aircraft cabins at high altitudes, to more earthly pursuits such as supplying oxygen to wounded soldiers in the field.

Solid oxide electrochemical cells have been used for many years in the extraction of oxygen from oxygen-bearing feed gases. The project under development implements a stack of electrolytic cells such that a large volume of oxygen can be produced. Toward this end, a 70-cell stack has been designed which fulfills the requirements of the project to be outlined below. A smaller stack of between three and five cells will be tested to determine the characteristics of such a design. These characteristics include, but are not limited to, thermal stress analysis, cycling time and amount of oxygen produced per square centimeter of active cell area.

Current oxygen generator technology is centered on evaluating and building devices using yttria-stabilized zirconia electrolytes. A series of studies for the United States Navy were just completed by Litton (#N62269-94-C-1283), Normalair Garrett Ltd. (#N62269-94-C-1285), United Technologies Hamilton Standard (#N62269-94-C-1284), and Sundstrand Aerospace (#N62269-94-C-1241) detailing conceptual designs for a ceramic oxygen generator for use in military aircraft. This work showed that conceptually, ceramic devices could be designed to deliver the required amount of oxygen in an aircraft.

Prior to this study DOE funded oxygen generator research and development at the Jet Propulsion Laboratory which resulted in the development of a small scale device ceramic generator. At the time of this program, however, there was little commercial interest in the development of these devices and the program was terminated after 2 years. Within the last several years there has been substantial commercial interest in ceramic oxygen generator technology for high volume production of oxygen that can be used in a large industrial process such as in steel, chemical, or glass plants. As a result R&D activities have increased in the area of electrolyzer materials and components. This increase in R&D activity has partially been driven by private studies that indicate that the use of ceramic generators may result in a significant cost savings by eliminating expensive blowers used in cryogenic oxygen generating systems. Solid oxide fuel cells are similar in design to oxygen generators, utilize essentially the same materials, and operate in the same temperature range to produce electricity. SOFC research and development has been

ongoing for 30 years and advances in this technology directly benefit oxygen generator development.

The proposed research and development program was to utilize solid oxide electrolytes to separate oxygen from air. The goal of the program was to develop a generator capable of delivering 4 liters/minute of pure oxygen at 30 to 40 psi. During the course of this program the deliverable was changed to a 3 to 5 cell stack, operating at 1000°C. This program was carried out primarily by Pacific Northwest National Laboratory (PNNL), and two subcontractors, the University of Arizona and Argonne National Laboratory.

2. Technology Description

The solid oxide electrochemical cell functions by ionizing oxygen at one electrode (cathode) and transporting these ions across a ceramic membrane (electrolyte) to a separate electrode (anode). This basic membrane structure is the heart of solid oxide fuel cell, oxygen sensors, catalytic membrane reactor, and oxygen generator technology.

A schematic diagram of the basic cell and reactions for an oxygen generator is illustrated in Figure 1. Typically, solid oxide cells operate in a temperature range from 500 to greater than 1000°C. An electrical potential is applied to the cell which promotes the transport of oxygen through the zirconia electrolyte. An electrochemical reaction at the electrode/electrolyte interface converts oxygen in the gas to oxygen ions in the crystal lattice of the electrolyte. The electrical potential from an external power supply provides the driving force to transport oxygen ions through the electrolyte. A reverse electrochemical reaction at the anode converts the oxygen ions to molecular oxygen.

The unique ability of zirconia to transport only oxygen ions provides the means for a high purity, compact oxygen generator. Oxygen ion vacancies created by the stabilizing dopant (yttria) are the source of oxygen transport. This transport phenomenon improves with temperature since the vacancies are more mobile at higher temperatures. The optimum operation temperature, for low power consumption, for doped zirconia is between 700 and 1000°C.

The current density through a driven membrane can be defined as:

$$j = \sigma_{eff} V_{eff} / t \qquad (1)$$

where j is the current density (A/cm^2), σ_{eff} is the conductivity of the cell (S/cm), t is the thickness and V_{eff} is the effective voltage. The conductivity (σ_{eff}) is thermally activated, increasing with temperature. V_{eff} can be defined as:

$$V_{eff} = V_a - V_n \tag{2}$$

where V_a is the applied voltage and V_n is the Nernst voltage which is defined as:

$$V_n = \frac{RT}{4F} \ln \left[\frac{PO_{2\ oxygen}}{PO_{2\ air}} \right] \tag{3}$$

where R is the gas constant, T is temperature (K), F is Faraday's constant, and $PO_{2\ oxygen}$ and $PO_{2\ air}$ are the partial pressure of oxygen and air, respectively. This equation shows that there is a direct dependence of the Nernst voltage on temperature and the oxygen partial pressures on both sides of the membrane. The Nernst potential must be overcome to drive oxygen through the membrane. Increase the temperature or oxygen partial pressure and the Nernst potential will increase.

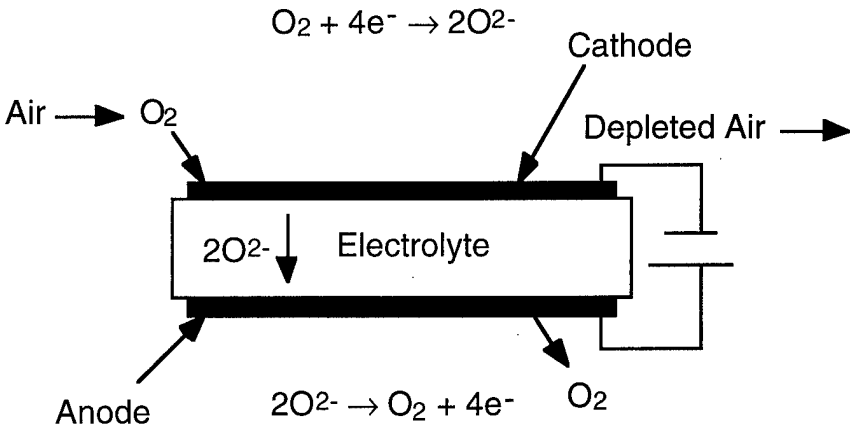

Figure 1 Oxygen Generator Reactions

2.1 Electrolyte Materials

Yttria stabilized zirconia is the best-known example of a solid electrolyte that conducts oxygen ions over a wide temperature range, is thermally stable, and exhibits reasonable mechanical properties. It is an oxygen ion conductor at high temperature with an electrical conductivity of 0.1 Siemans/centimeter (S/cm) at 1000°C. In general, fully stabilized, 8 to 10 mole percent Y_2O_3, YSZ is preferred as an SOFC electrolyte in order to maximize conductivity. The use of fully stabilized YSZ avoids problems of phase transformation associated with partially stabilized materials during cell operation. This material has been widely researched and is recognized as the current material of choice for high-temperature oxygen separation applications.

Substantial improvements in performance, operation temperature and oxygen flux, can only be obtained by changing the electrolyte material. There are other metal oxides that offer higher oxygen ion conductivities than yttria stabilized zirconia; these include scandia-stabilized zirconia, lanthanum gallate, ceria, and bismuth oxide. Scandia-stabilized zirconia [1] exhibits greater ionic conductivity than yttria-stabilized zirconia between room temperature and 1000°C. Its high cost, however, is a disadvantage and would prevent use and acceptance of this material except in thick film applications.

Cerium oxide (CeO_2) offers higher ionic conductivity than YSZ when appropriately doped with trivalent acceptor cations (e.g., Sm^{3+}, Gd^{3+}). In the 600-800°C temperature range, the conductivity of doped ceria is approximately 2-3 times that of YSZ. Because of the high ionic conductivity doped ceria is a candidate to reduced temperature oxygen generation. The principle uncertainty of using doped ceria is its high thermal expansion coefficient (ceria ≈13-14 ppm/°C, YSZ ≈10.5 ppm/°C).

Lanthanum gallate ($LaGaO_3$) [2-4] offers higher ionic conductivity than YSZ when appropriately doped with divalent acceptor cations (e.g., Sr^{2+} and Mg^{2+}). Similar to doped ceria, the conductivity of lanthanum gallate approximately 2-3 times that of YSZ in the 600-1000°C temperature range. The enhanced conductivity in lanthanum gallate is attributable both to a higher concentration of oxygen vacancies and a higher mobility of those vacancies relative to YSZ, with the increased mobility making the largest contribution. As in the case of YSZ, electronic conductivity is very low, so that the ionic transference number approaches unity. Gallate powders prepared by appropriate synthesis techniques are readily sinterable to high density (greater than 97% of theoretical) at moderate sintering temperatures (1400-1500°C). The thermal expansion coefficient is approx. 12 ppm/°C,

which is somewhat higher than that of YSZ. The fracture strength of sintered lanthanum gallate (approx. 150 MPa) is relatively constant up to 1000°C.

Stabilized bismuth oxide, Bi_2O_3, offers the highest ionic conductivity among solid oxide electrolyte candidates. In the 500-700°C temperature range, the conductivity of stabilized Bi_2O_3 can exceed that of YSZ by 1 or 2 orders of magnitude. Stabilization of the desired δ-Bi_2O_3 structure is accomplished by doping with appropriate cations, e.g., Y^{3+}. The very high ionic conductivity makes Bi_2O_3 an attractive candidate for low temperature oxygen separators, but other factors must be considered. One particular disadvantage of Bi_2O_3 is its limited stability under reducing conditions. For example, stabilized Bi_2O_3 readily reduces in the presence of a modest potential. Another potential disadvantage of Bi_2O_3 is its low melting point, significant fabrication challenges may have to be overcome in order to prepare generator stacks incorporating Bi_2O_3 electrolyte membranes with more refractory electrode and interconnect materials.

Table 1 indicates the advantages in terms of membrane thickness and operating temperature that can be obtained for several electrolytes. The ionic conductivity and thus performance of lanthanum gallate at separating oxygen at 700°C can only be matched by yttria stabilized zirconia operating at 1000°C (Table 1). This clearly indicates that by replacing yttria stabilized zirconia with lanthanum gallate, the operating temperature of the device can be lowered from 1000°C to 700°C. Further reduction in the operation temperature can be achieved by reducing the electrolyte thickness to ≈50 μm as shown in Table 1.

The selection of the electrolyte material is critical for reliable operation of the oxygen generator. The selection criteria for the electrolyte are:

- High ionic conductivity, transference number of 1
- Stability in oxidizing environments
- Chemically compatible with other generator materials
- Sinterable to full density
- High mechanical strength
- Easily fabricated into thin sheets

Currently, only 8 mole % yttria-stabilized zirconia satisfies all these requirements and therefore, it was chosen as the electrolyte for this development program.

Table 1. Thickness (μm) required to yield the same resistance per cm^2 as 200 μm thick yttria stabilized zirconia at 1000°C.

Composition	Thickness (μm) at Temperature				
	600 °C	700 °C	800 °C	900 °C	1000 °C
$La_{0.9}Sr_{0.1}Ga_{0.8}Mg_{0.2}O_3$	50	120	200	500	800
CeO_2 + 5 m% Y_2O_3	50	120	200	500	800
Bi_2O_3 + 25 m% Y_2O_3	200	400	800	----	----

2.2 Electrode Materials

The electrode material must meet the following criteria:

- high electrical conductivity at the operating temperature
- chemically stable and compatible with the electrolyte
- thermal expansion match to electrolyte
- low polarization

Extensive studies were carried out previously to evaluate the relative advantages of other electrode materials over Sr-substituted lanthanum manganite (LSM), which was previously used for the base line in past studies [5]. Examination of the literature of the properties of LSM and LCM as well as detailed studies were used to determine which material to use as the electrode and material for the separator plate. Based on its close thermal expansion match to yttria-stabilized zirconia (Figure 2), $La_{0.8}Ca_{0.2}MnO_3$ was chosen as the material to develop in this program.

2.3 Separator Plate Materials

The separator plate in the oxygen generator performs the task of gas manifolding, electrical current distribution, and it provides the mechanical support necessary for the thin electrolytes to withstand the stress loading of the stack. The requirement for a high-temperature separator plate are:

- Stability (chemical, phase, microstructural, dimensional) at 1000°C in an oxidizing atmosphere
- High electrical conductivity
- Thermal expansion match to yttria stabilized zirconia

- Minimal chemical interaction with the electrolyte
- Sinterable to full density to prevent oxygen transport
- High mechanical strength and toughness
- Low cost
- Easily fabricated

Since the generator does not see severely reducing environments, a LCM separator will be used in this application. Since LCM is also used as the electrode materials, compatibility is not an issue in the generator under development in this program. The use of LCM also offers the possibility of better seals between the separator plate and the electrolyte due to their close thermal expansion match (Figure 2).

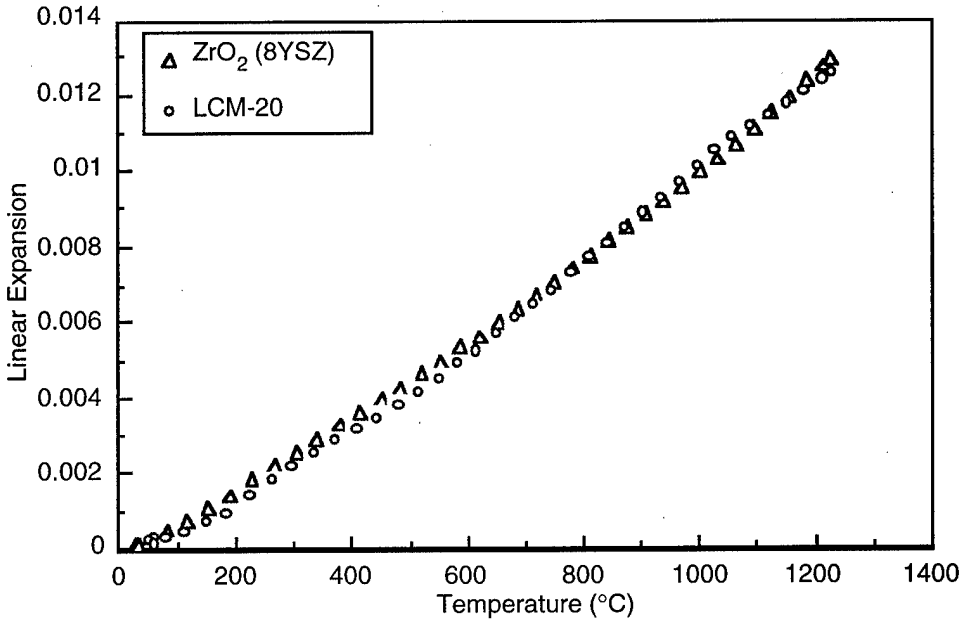

Figure 2. Linear expansion of 8 mole percent yttria stabilized zirconia and $La_{0.8}Ca_{0.2}MnO_3$.

2.4 Design

2.4.1 Design Parameters

The basic requirements for this project was to design and build a portable oxygen generator, capable of producing oxygen at a rate of 4 liters per minute (l/min) at a delivery pressure of 30 psig. The unit must be self contained, except for power supply and be able to be ramped up to operating conditions in a reasonably short time.

Oxygen generation is based on solid oxide electrolysis, a process in which oxygen atoms are conducted through a ceramic electrolyte and thereby separated from the feed gas. This process is operated at a temperature of 1000°C. The amount of oxygen generated per electrolyte area is limited by surface area and kinetics. For large oxygen output rates, it is not practical to build one large stack. Instead a modular approach is advised. Modular stacks can provide a smaller overall volume of the oxygen generator, guaranteeing higher reliability, and offer fabrication advantages.

2.4.2 Cell and Stack Design

Figure 3(A) and Figure 3(B) illustrate, from top to bottom, a separator plate, a seal, an electrolyte plate, a seal, and a separator plate. This comprises one complete building block (i.e. single cell) of the stack which can then be added to other blocks to form the 70-cell stack.

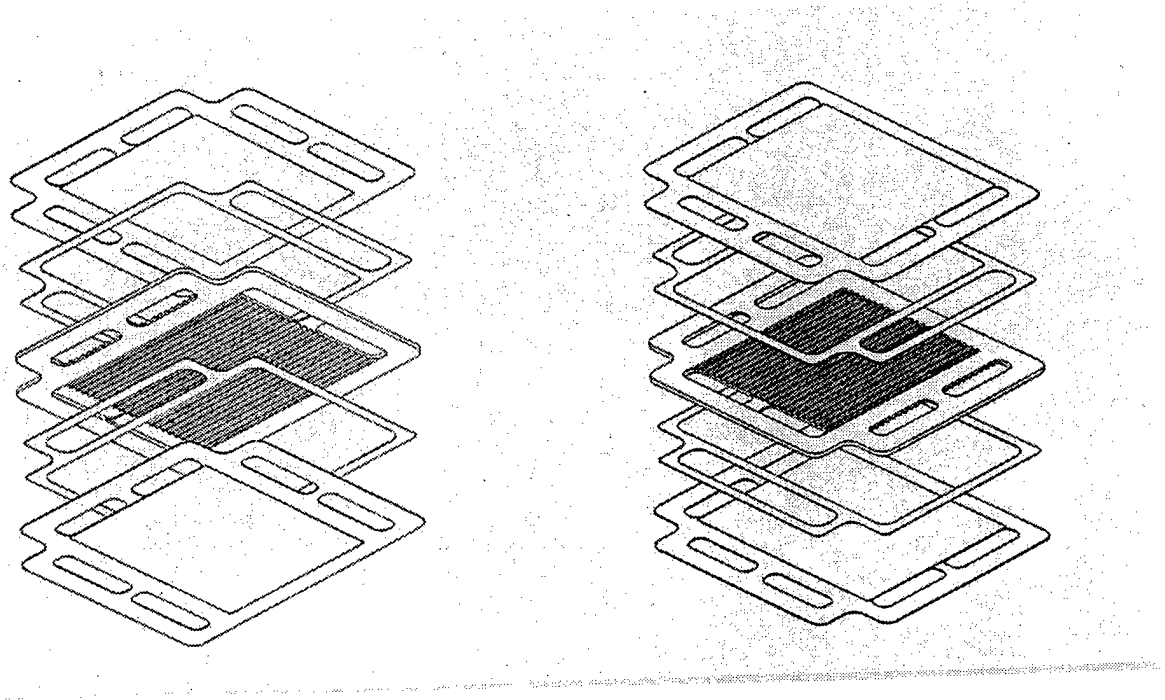

Figure 3. Module assembly: (A) air side, (B) oxygen side.

Air is drawn into the stack, and each block, as illustrated in Figure 4. The ribs running along each side of each interconnect plate are orthogonal. Incoming air is guided from left to right over the top face of the electrolyte. Outgoing oxygen is guided along the bottom of the electrolyte and exits at the front of the stack as shown in Figure 4. Gases from each individual cell are collected in the vertical channels on the left, right, and front of this

illustration. Only three streams of gases have to be interfaced to the stack, which is important for the efficiency of the thermal insulation of the stack.

3. Fabrication Technology

3.1 Electrolyte Fabrication

The 8 mole% yttria stabilized zirconia electrolytes were fabricated by tape casting. Tape casting is a fabrication process for forming large area, thin flat ceramic layers. The tape casting process starts with a slip (or slurry) of ceramic materials. The slip contains organic binders, plasticizers, and dispersants dissolved in an organic solvent system. The slip is spread on a flat surface to a controlled thickness with the knife edge of a doctor blade, and the solvents are allowed to evaporate in a controlled manner to minimize stresses that may

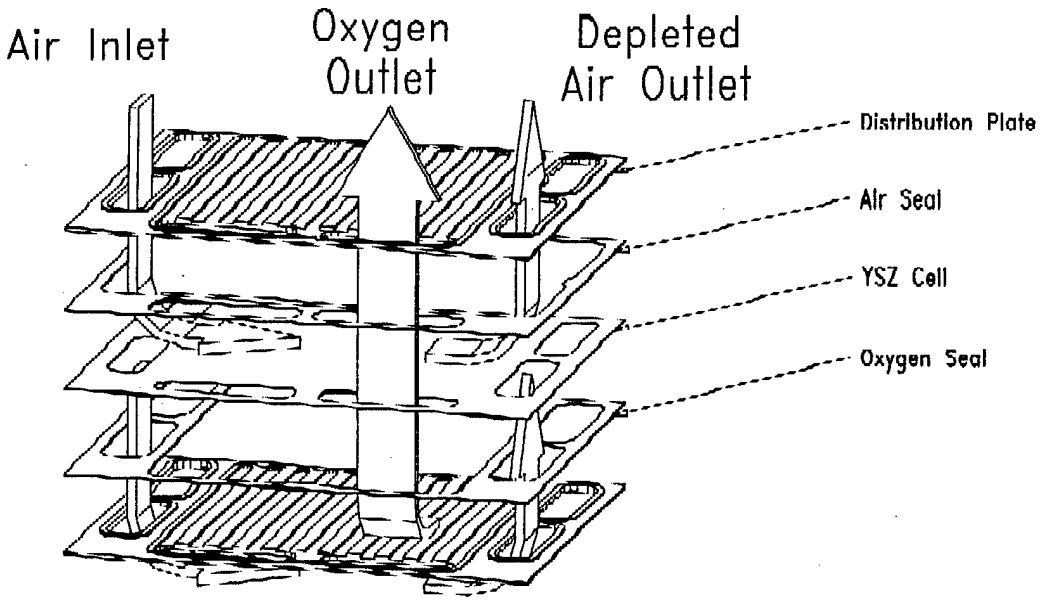

Figure 4. Flow Diagram

arise from differential shrinkage. The resulting dried tape, containing oxide powders and plastic binders, is flexible. It can then be stripped from the casting surface, cut to size or otherwise formed prior to firing. For the purpose of this program, the electrolytes were procured from an outside vendor. PNNL purchased approximately 50 plates which had density of 96 to 97 percent of theoretical (Figure 5). These cells are approximately 200 μm

thick, with a 50 μm thick LCM electrode applied to both sides. The electrode active area is approximately 25 cm^2 covering the ribs on the separator plate.

3.2 Electrode Fabrication

The LCM electrodes were deposited by screen printing. LCM powders were mixed with a organic solvent and binder system using a three-roll mill. The powder and binder were mixed until a homogeneous paste was obtained, approximately 5 to 10 minutes. The paste was placed onto a patterned screen and forced onto the electrolyte surface using a squeegee. The printed inks were dried at 50°C in air and then the process was repeated on the other side of the electrolyte. The printed electrodes had a thickness after binder removal and sintering of ≈50 μm. A typical sintered electrode microstructure is shown in Figure 6.

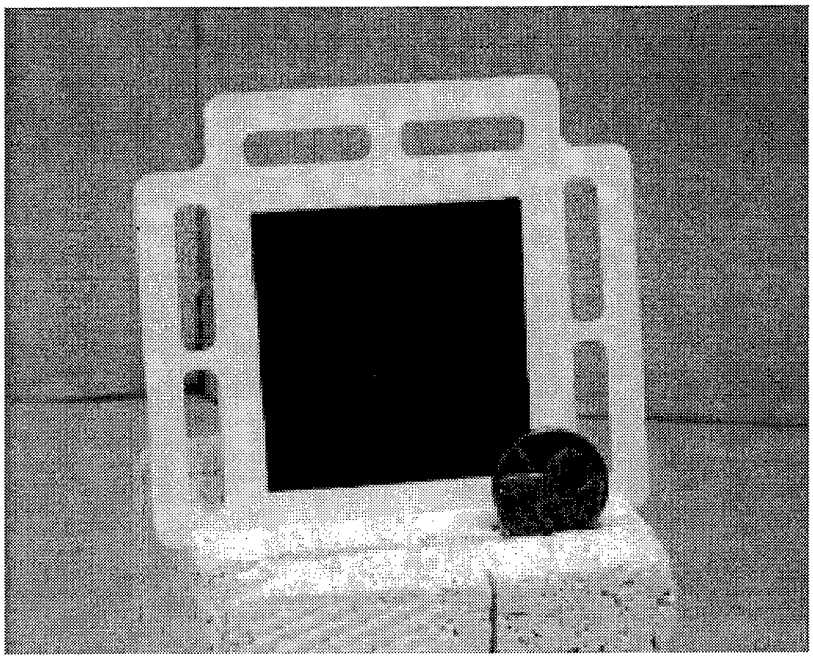

Figure 5. Typical electrolyte plate with printed electrode.

3.3 Separator Plate Fabrication

The fabrication of separator plates for oxygen generators or solid oxide fuel cells has been a perennial challenge facing developers. Pressing, tape casting, and tape calendering are processes that are typically utilized to fabricate separator plates or interconnects for the various device designs [6,7]. The selection of a suitable fabrication process is highly dependent upon the device design. In addition, the raw material properties, such as surface area, particle size and distribution, and morphology affect the processing parameters. The

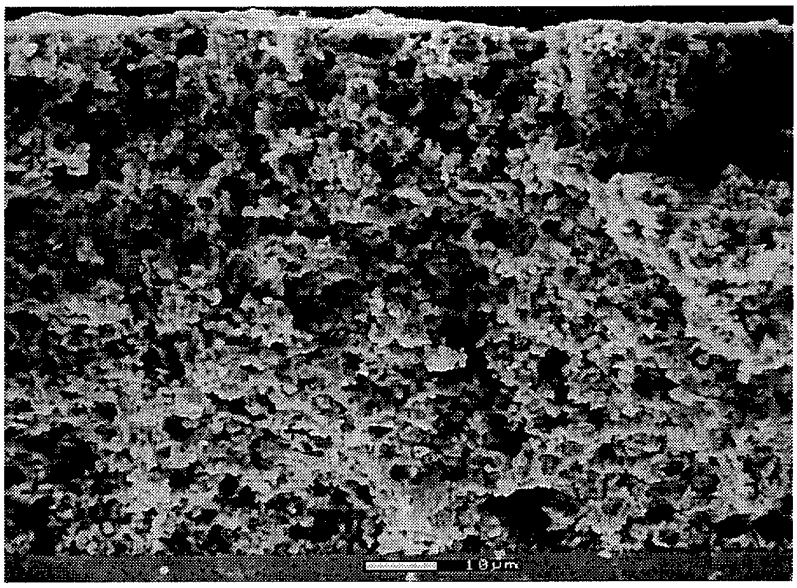

Figure 6. Typical screen printed electrode (after sintering) on stabilized zirconia electrolyte.

influence of the initial powder characteristics on consolidation of ceramic powders has been well studied [8,9].

Traditionally, separator plates for solid oxide fuel cells have been made by hot pressing lanthanum chromite at high-temperature to form a dense flat plate, as detailed in Figure 7. The proper vias and flow channels are then machined into the plate. This is a costly process and not practical for large scale production of components.

PNNL has develop a low cost approach to the fabrication of separator plates. This technology utilizes molding technology to fabricate the separator plate. For this process the LCM powder was thoroughly mixed with approximately 10 weight percent of an organic binder. The binder powder mixture was placed into a die and uniaxially compressed at 150°C for 10 minutes. After pressing the die was cooled and the part removed. The pressed parts were slowly debindered and then sintered to full density (1450°C/2 h) (Figure 8).

3.4 Manifold Fabrication

Manifolds were made by slip casting thick plates of 8 mole percent yttria stabilized zirconia. After the plates were dried, they were sintered to full density (1400°C/2hr) and the surfaces machined flat. Two plates (top and bottom) were needed for each stack to be assembled

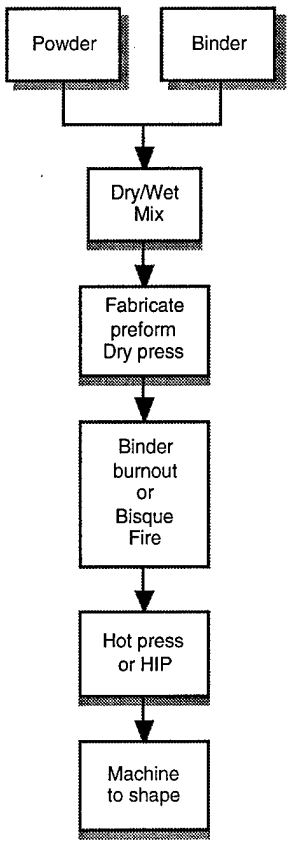

Figure 7. Flow chart of interconnect plate manufacturing process.

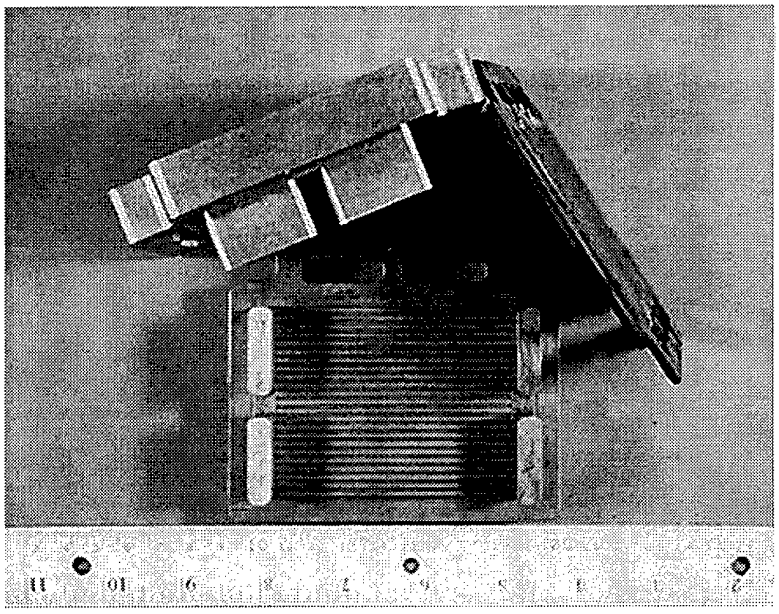

Figure 8. Picture of die and pressed separator plate.

and tested. In the top plate, holes were drilled for the air inlet, air outlet, oxygen outlet and for the current/voltage lead attachment. No holes were machined in the bottom plate.

4. Seal Development

Seal design and development has been a major issue. Appropriate materials and designs have not yet been developed reliability to form seals which can be made leak tight and maintained through repeated thermal cycles, without chemical interaction with the other cell components, or failure. The major activity during this project was the development of an appropriate seal material which would prevent cross contamination of the gas streams. Several candidate materials, both glass and metallic, were evaluated at Argonne National Laboratory (ANL) and PNNL.

4.1. Characterization of Seal Materials

Two glass samples, glass K and glass 43, were received from Argonne in July 1996. Glass K was assigned lot number KPNL01, glass 43 was designated as 43PNL01. Glass K is the main seal material developed by ANL to seal high-temperature solid oxide fuel cells, while glass 43 is the fluxing material used to lower the melting point of glass K. During the program, it was difficult to obtain enough sealant to carry out sealing tests to check for compatibility with the stack materials and design. New lots of glass sealant were synthesized at PNNL. For PNNL to accurately reproduce the glass sealant, it was necessary to verify or determine their compositions. Therefore, chemical analysis was carried out on both glass samples using ICP and EDX qualitative analysis. The analyzed compositions are reported in Table 2.

Table 2. Composition of glasses prepared at ANL.

Oxide Component	Glass K Composition (Lot KPNL01)				Glass 43 Composition (Lot 43PNL01)			
	Reported by ANL		Analyzed		Reported by ANL		Analyzed	
	Mole%	Wt%	Mole%	Wt%	Mole%	Wt%	Mole%	Wt%
B_2O_3	36.6	19.0	35.75	18.75			33.3	26.3
La_2O_3	20.2	49.1	19.51	47.89			3.0	11.1
SrO	28.7	22.2	38.61	30.14			26.8	31.5
SiO_2	4.6	2.1	4.74	2.15			20.3	13.8
Al_2O_3	10.0	7.6	1.39	1.07			16.6	19.2

During the course of the program PNNL synthesized batches of glass K and glass 43 in order to have sufficient quantities available for sealing studies. The composition of the glasses synthesized are reported in Table 3. The composition of the synthesized material is close to the composition reported by ANL and those determined by quantitative analysis of ANL' s powder. Within the limits of experiment error, there is remarkable equivalence in chemistry between similar glasses prepared by ANL to those prepared by PNNL.

Table 3. Composition of glasses prepared at PNNL

Oxide Component	Glass K Composition (Lot KPNL03)				Glass 43 Composition (Lot 43PNL02)			
	Nominal		Analyzed		Nominal		Analyzed	
	Mole%	Wt%	Mole%	Wt%	Mole%	Wt%	Mole%	Wt%
B_2O_3	35.75	18.75	36.3	19.8	33.3	26.3	33.2	26.0
La_2O_3	19.51	47.89	17.6	44.9	3.0	11.1	2.7	9.9
SrO	38.61	30.14	37.7	30.6	26.8	31.5	24.8	28.9
SiO_2	4.74	2.15	5.9	2.8	20.3	13.8	21.4	14.5
Al_2O_3	1.39	1.07	2.5	2.0	16.6	19.2	18.0	20.7

4.1.1 Crystalline Phases in Glass K and 43

Glass 43 was completely amorphous after preparation, while glass K (K-PNL01) contained approximately 50 vol% crystalline phases. The crystalline phase is composed of two forms of $LaBO_3$ (80 wt%), while the remaining 20 wt% has yet to be identified. X-ray analysis was carried out on both the as-received glasses from ANL and those prepared by PNNL.

Glass 43 prepared at PNNL (Lot 43PNL2) was also completely amorphous, while the PNNL glass K (Lot KPNL3) had the same crystalline phase content (80 wt%) as the ANL glass. Glass K, however, has different crystalline phases present. Since no heat treatment was applied to this glass after synthesis (i.e. ANL did not indicate the thermal history for the glasses they delivered) the difference may be due to annealing the glass at high-temperature to develop the proper phase distribution.

4.1.2. Crystallization Behavior

In order to determine the correct thermal schedule for sealing, the softening and crystallization behavior of glass K was studied. Glass K showed a major crystallization event between 220 to 280°C and a second crystallization event between 700 and 720°C.

When glass K was mixed with 10 wt% glass 43, the mixture showed a single crystallization peak between 700 and 720°C.

4.2. Sealing Studies

4.2.1. Procedure

8 mole% yttria stabilized zirconia disks (20mm diameter, 0.5 to 2 mm thick) were used as substrates for the sealing studies. Glass K was mixed with an organic vehicle to make a slurry, brushed onto the substrates, and air dried for 30 minutes. The two zirconia disks were sandwiched together and heated to observe the sealing process. Heating and cooling rates were controlled from 5°/min to 200°C/min for temperatures from 1000 to 1350°C. General results and observations of the sealing tests are listed in Appendix A. Appendix B contains optical and scanning electronic microscopy analysis of the glasses and seal tests.

Based on observations from the glass K sealing, it was apparent that a lower sealing temperature was required to form a hermetic seals. Therefore, glass 43, a low melting glass, was mixed with glass K to effectively reduce the softening temperature of the seal material. Samples were prepared as before by forming a slurry of the glass mixture with an organic which was painted onto the stabilized zirconia substrates for testing. For these studies the heating rate was held constant at 1°C/min.

4.2.2. ZrO_2 Substrates

Based on the studies carried out adequate seals between two zirconia disks were obtained with 10 and 20 weight percent addition of glass 43 to glass k when sealed at 1000 and 1050°C.

Table 4. Effect of Glass 43 on Sealing Quality and Temperature of ZrO_2

Seal Temperature (°C)	Glass K+0 wt%43	Glass K+10 wt%43	Glass K+20 wt%43
950°C	S, IMF, Fig 9A	S, MMF, Fig 9B	S, MMF, Fig 9C
1000°C	S, IMF, Fig 9D	S, MMF, Fig 9E	S, **AMF**, Fig 9F
1050°C	S, IMF, Fig 9G	S, MMF/**AMF**, Fig 9H	S, **AMF**, Fig 9I

S = sealed; AMF = adequate melt flow; MMF = marginal melt flow; IMF = inadequate melt flow; EMF = excess melt flow

4.2.3. LCM Substrates

Table 5. Effect of Glass 43 on Sealing Quality and Temperature of LCM

Seal Temperature (°C)	Glass K+0 wt%43	Glass K+10 wt%43	Glass K+20 wt%43
970°C	----	S, AMF, Fig 10A	S, AMF, Fig 10B
1000°C	----	S, AMF, Fig 10C	S, AMF/EMF, Fig 10D
1050°C	----	----	----

S = sealed; AMF = adequate melt flow; MMF = marginal melt flow; IMF = inadequate melt flow; EMF = excess melt flow

Based on the studies carried out adequate seals between two zirconia disks were obtained with 10 and 20 weight percent addition of glass 43 to glass k when sealed at 970 and 1000°C.

4.3 Modified Seal Material

The primary objective of this study was to determine if additions of LCM to the seal material would:

- Increase chemical compatibility at the seal interface and reduce corrosion of LCM substrates by boron in the glass. The addition of LCM was anticipated to partially dissolve in borate glass and pre-saturate it with CaO.
- Enhance thermal compatibility and reduce stress related cracking at the seal interface.

Table 7 summaries the measured and predicted thermal expansion coefficient for a series of sealant mixtures consisting of glass 43, glass K and LCM. The predicted values are usually in agreement with the measured value. A discrepancy was observed when the mix contains large amounts of LCM and glass 43.

The stability of LCM, when in contact with glass K and 43, was examined using thermal gravimetric analysis. A mixture of glass 43 and LCM (TE-50) show a large weight loss upon heating. This was believed to be caused by the reduction of LCM during heating in the presence of glass 43. TGA analysis of glass 43, without any added LCM, shows no loss in mass with temperature. The addition of glass K to the LCM and glass K mixture (TE7) resulted in less interaction and less loss of mass during heating.

Table 6. Density and Thermal Expansion Coefficients of Baseline Materials

	Glass 43	Glass K	LCM
Density (g/cc)	3.14	4.33	6.27
Thermal Expansion Coefficient (10^{-6} C^{-1})	7.3	12.55	10.5

Table 7. Modeled and Experimentally Determined Thermal Expansion Coefficient for a Variety of Seal Compositions

Sample Identification Number	Glass 43 (wt%)	Glass K (wt%)	LCM (wt%)	Modeled Thermal Expansion Coefficient (10^{-6} C^{-1})	Measured Thermal Expansion Coefficient (10^{-6} C^{-1})
TE5	8.0	72.0	20.0	11.7	11.9
TE6	8.0	52.0	40.0	11.3	11.0
TE7	12.0	68.0	20.0	11.5	12.0
TE8	12.0	48.0	40.0	11.1	9.8
TE12	10.0	90.0	0.0	12.0	12.0
TE15	20.0	80.0	0.0	11.5	11.0
TE16	100.0	0.0	0.0	7.3	7.3
TE13	13.3	86.7	0.0	11.9	11.9
TE17	0.0	100.0	0.0	12.6	12.6
TE50	50.0	0.0	50.0		

4.4. Conclusions

1. The initial sealing trials with glass K were encouraging:
   - glass K seems to bond well to 8 mole% yttria stabilized zirconia at temperatures as low as 1000°C.
   - Optical and SEM examination of the seals indicates good bonding and good mechanical integrity
2. Introduction of a lower temperature glassy phase (glass 43) is beneficial:
   - The sealing temperature can be adjusted by varying the concentration of glass 43. For this study, 10 wt% of glass 43 is adequate for sealing both zirconia to zirconia and LCM to LCM.
3. Sealing trials with glass k and 43 easily sealed small coupons of zirconia to LCM:

- Scale-up to large seals for the stack difficult.
- Seal scale-up included tape casting as a method to make the large seals
- All attempts to seal the large cells with glass k or glass k mixed with glass 43 resulted in fracture of the stack. This was thought to be caused by stresses arising from different thermal expansion coefficients.
- In no instance during this project was PNNL able to seal a full scale zirconia cell to LCM separator plate using these seal materials.

4. Initial observations of seals containing LCM, in addition to the glass, indicated enhanced seal integrity to LCM substrates. However, the thermal mechanical compatibility of the seal to ZrO_2 substrate decreased.

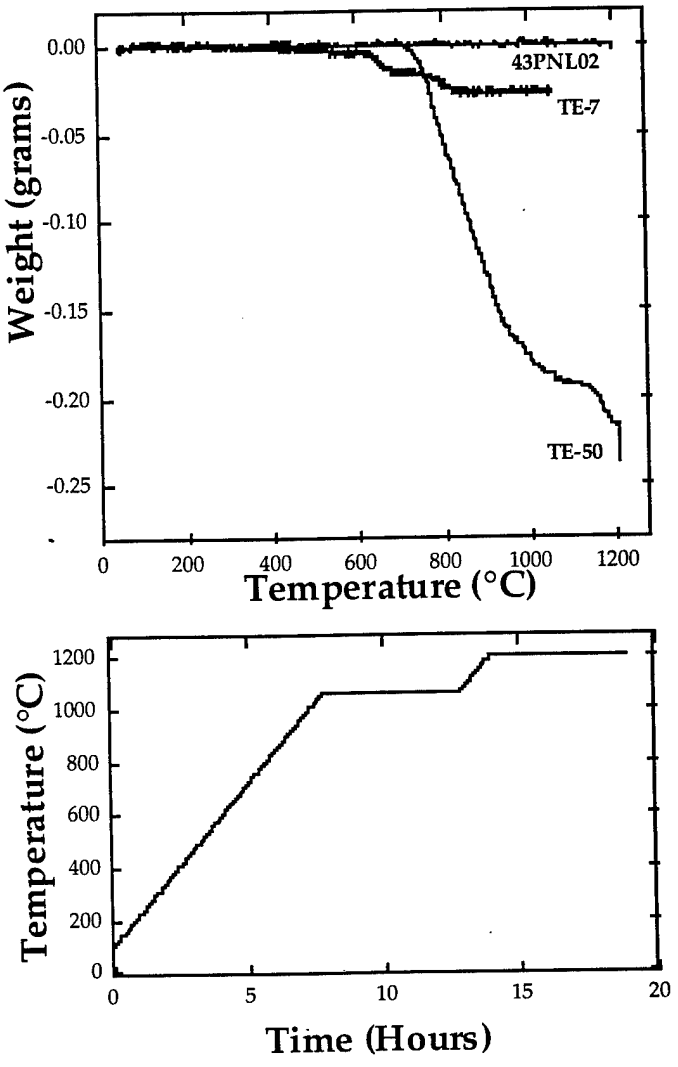

Figure 9. Plot of weight loss as a function of temperature for several glass seal compositions.

5. Oxygen Generator Hardware

5.1 Balance of Plant

Testbeds have been built for both the smaller stack design and the single cell modules. An electronic control box was constructed capable of controlling the full 70-cell stack. This control unit will be used in powering the heaters, collecting cell voltage and current data as well as measuring air and oxygen flows through the three to five cell stack and the 70-cell stack. A complete testing system for both single cell modules and a small stack of solid oxide electrochemical cells has been developed.

5.1.1 Stack Support

The full design of the portable oxygen generator requires a stack of ≈70 8 mole% yttria stabilized zirconia cells and associated interconnect plates. As the stack is ramped up to operating temperature, all of these parts will expand and shift slightly when the glass seal begins to heat up. Therefore, the entire stack must be constrained in some fashion, as illustrated in Figure 10. Across the top and bottom of the stack, titanium brackets are held in place with inconel springs, tie rods, nuts and washers. The support exerts a slight pressure, just enough to overcome the 30 psig differential inside the stack. All components are held securely in place, with no possibility of movement.

Removing the brackets and heaters from the stack in Figure 10 exposes the 70 cells, manifold plates and heaters surrounding these cells, as seen in Figure 11. Rather than connect all 70 cells in series, three separate modules were designed to house approximately 1/3 the full complement of the stack. This was done to protect against a failure in one or more individual or interconnect plates, which would result in failure of the complete stack. If one component should fail, 2/3 of the entire stack will still produce oxygen.

5.1.2 Stack Thermal Insulation

The stack insulation for this project needed to withstand an interior temperature of 1000°C on the outer surface. Only materials with a very low thermal conductivity can accomplish this within a small overall packaging size. Min-K was chosen since it has an extremely low thermal conductivity and is easy to shape. A heat conduction analysis showed that the insulation needed to be approximately 1 inch thick.

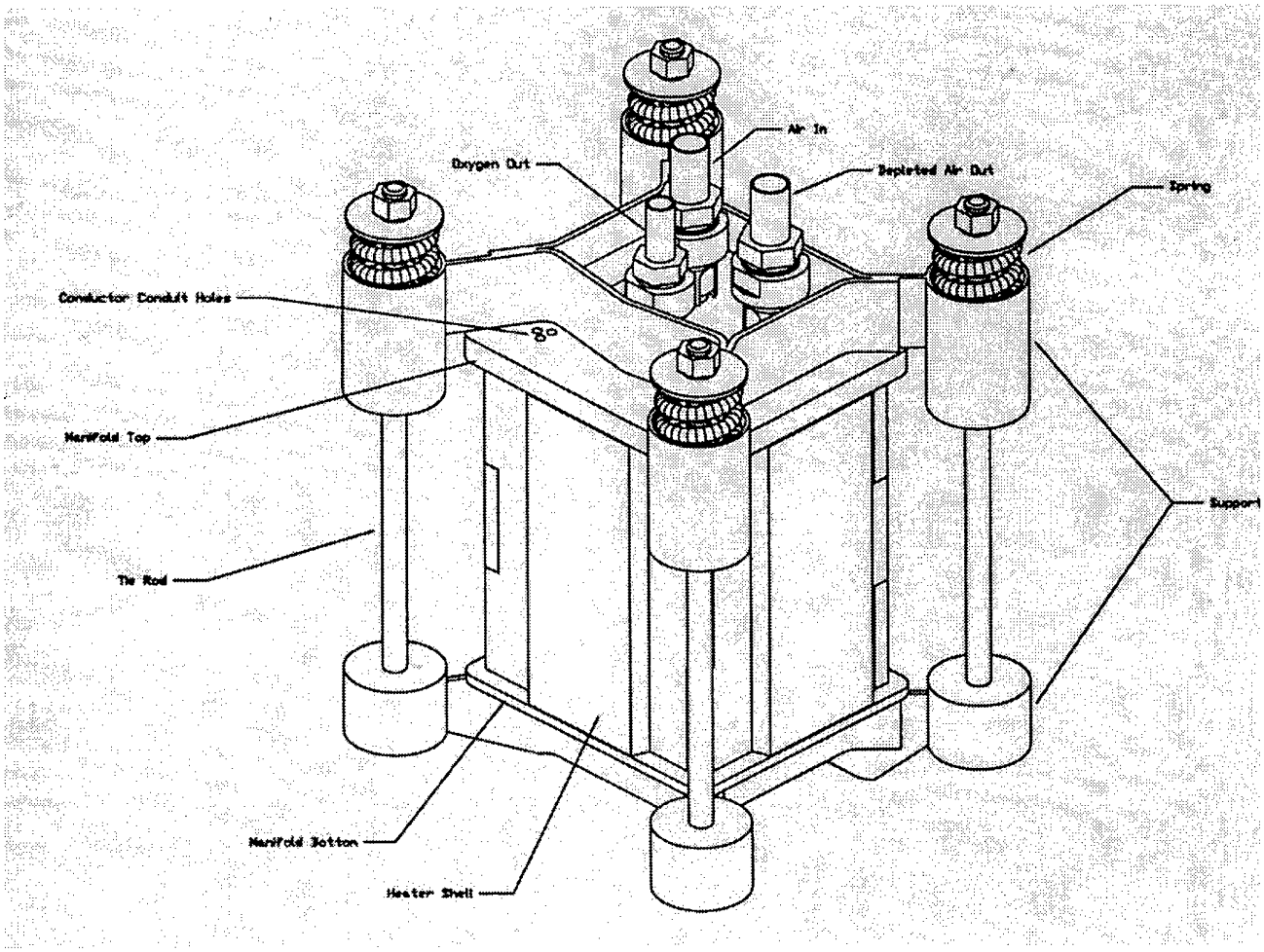

Figure 10. Assembled 70 cell stack

5.1.3 Stack Heaters

The cell stack must be heated at a relatively slow ramp rate to avoid damage to the cell stack. The size of the heaters was also a concern. Since off-the-shelf heaters are fairly large and thick, heaters manufactured in-house were being used. These were constructed of an A-Lava body and machined out to accept Kanthal heating element wire, which was spiral wound in-house.

The A-Lava is a machinable ceramic-type material which, after firing, can withstand the operating temperatures of this stack. As seen in Figure 11, these heaters are locked together upon assembly by simply aligning the tags and notches, thus providing a functional, compact design. Previous trials at the University of Arizona have proven Kanthal AF heating wire to be a very reliable source of heat.

Each heater was supplied with 120 VAC and was wired in series to produce approximately 500 W to the stack. Ramp rate of the heaters, as well as set point and thermocouple monitoring was controlled by a heater controller mounted in the control box.

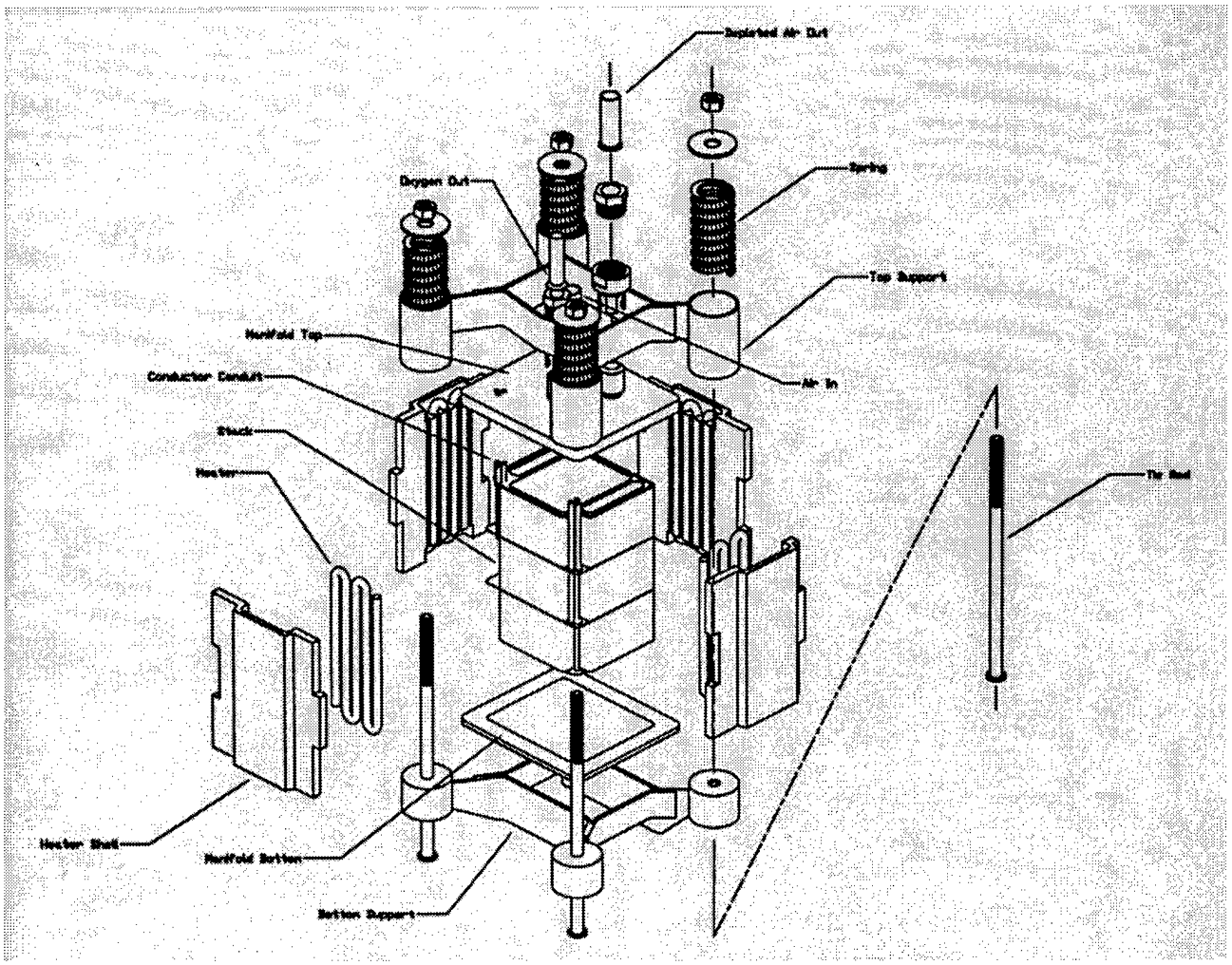

Figure 11. Stack assemble exploded view.

5.1.4 Air Flow Generation

For a given temperature and current, the limiting flow rate of the feed gas (air) is defined as the amount of air to supply all the oxygen that can be pumped across the membrane if all the oxygen is scrubbed from the air. Any feed gas greater than this value is excess and is exhausted in the exhaust stream. If the flow is less than this limit, cell performance will be reduced due to lack of oxygen. The electrolyte could eventually become damaged if the DC voltage potential across the cell is maintained at levels comparable to the breakdown potential for stabilized zirconia, due to stripping of oxygen from its own structure. The actual mass flow rate of oxygen in the feed gas will be greater than the amount being

pumped across the electrolyte at the mass limiting condition. This is needed to overcome the concentration gradients at the surface of the disk.

A diaphragm air pump was selected for the project. Diaphragm air pumps are more stable than other pump designs and provide a constant flow at a constant pressure. Diaphragm pumps also do not contaminate the air flow with oil, debris, or leakage; which provides a controlled set of conditions for data collection. The pump selected delivers 37.7 l/min at a gage pressure of 0.3 bar.

5.1.5 Operational Controls

Air into the stack was controlled electronically, and oxygen out of the stack was monitored electronically, as seen in Figure 12. A check valve, pressure transducer and flow regulator assured proper back pressure within the stack, as well as providing a safety measure to protect against any possible pressure overloads on the system. An oxygen storage tank was utilized to provide a buffer between the oxygen outlet on the front panel of the control unit and the stack. Inlet and outlet ports were located on the front panel of the control unit (Figure 13). Also seen in Figure 13 is the heater controller, module jacks and thermocouple inputs. All internal components, as built, can be seen in Figure 14.

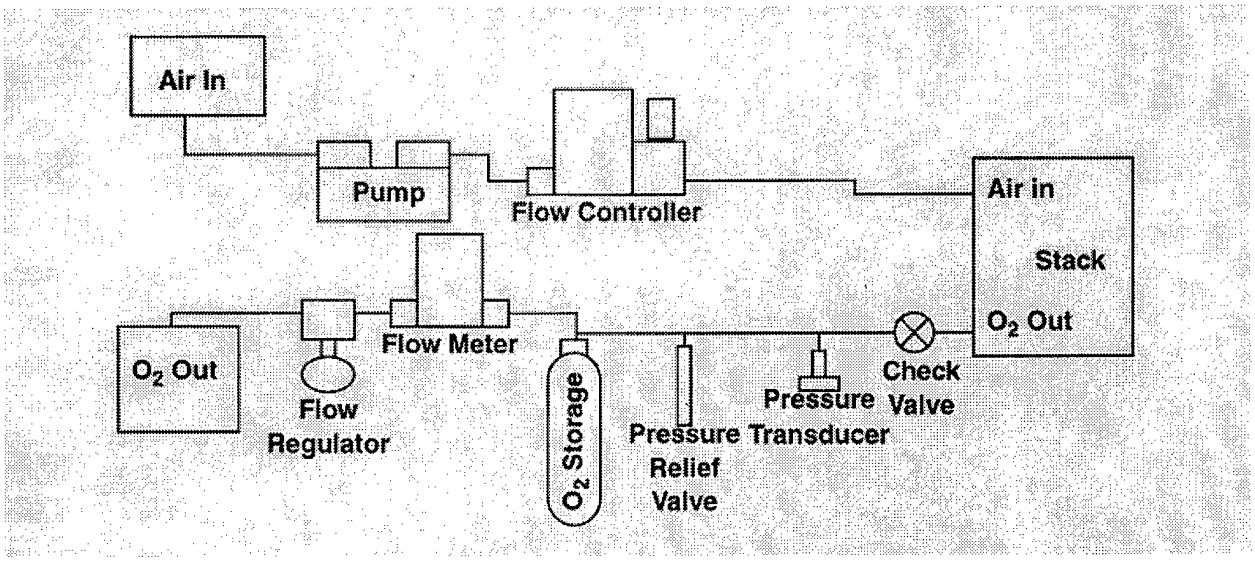

Figure 12. Oxygen generator schematic.

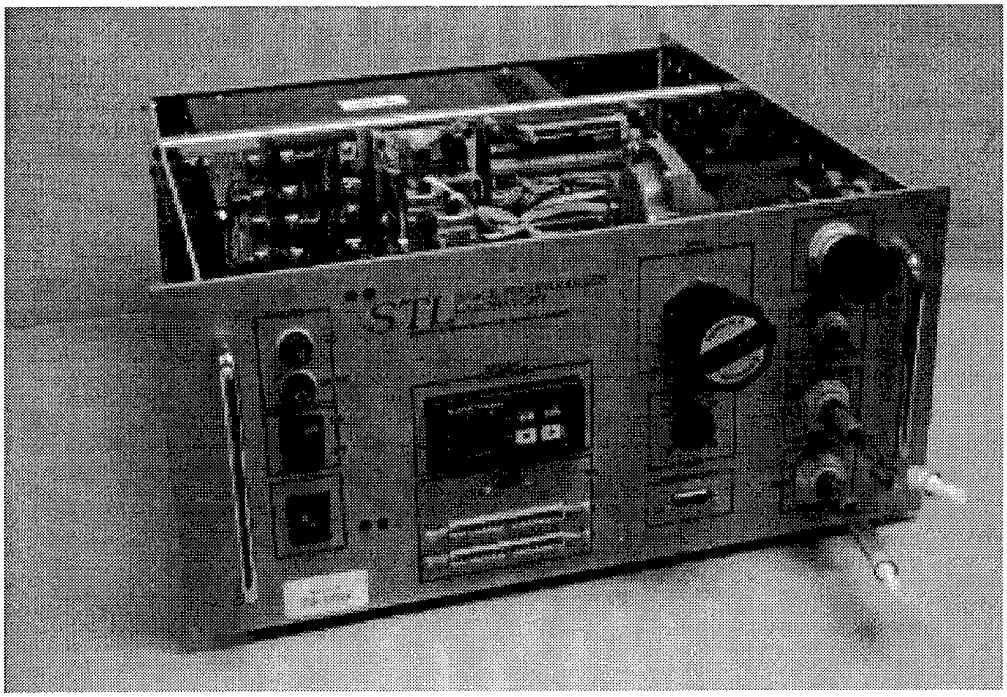

Figure 13. Control housing.

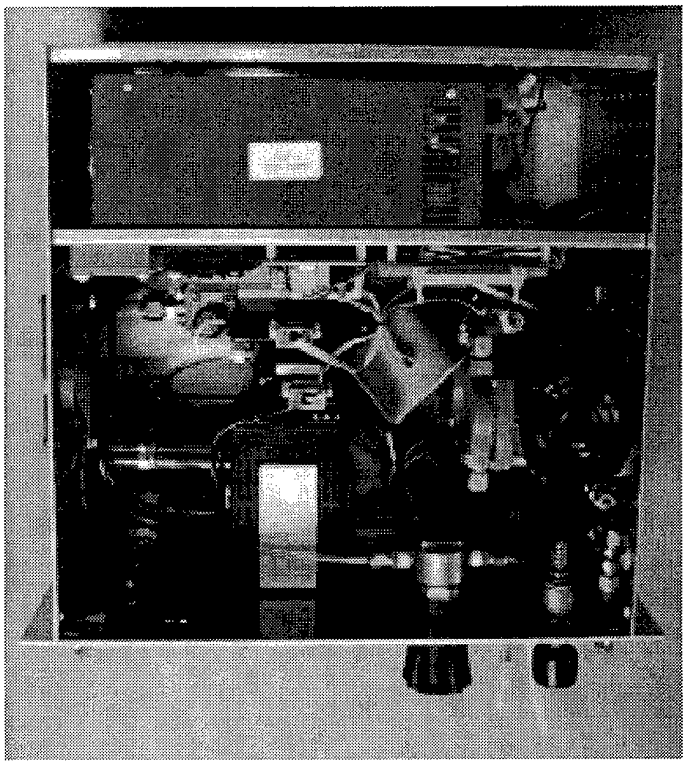

Figure 14. Electronic Components.

The interior panel of the control box contained two I/O blocks for connection to the data acquisition cards, a DC power supply to operate the flow meter and flow controller, fuses, and various connectors. Also on the panel was a bank of AC solid state relays to control the heaters, fans, and pump, as well as three DC sold state relays to operate the stack. A large DC power supply was located behind the interior panel. This power supply provides power to the cell stack. High current requirements necessitated a 45A, 0-18V supply.

5.1.5.1 Air Flow Controller

The flow controller was connected to the computer via one of the digital inputs on the data acquisition cards. Maximum volume flux for the controller was 50 sl/min.

5.1.5.2 Thermal Controller

The thermal controller on the main panel monitored the stack temperature with one of the type K thermocouples in the thermocouple bundle. This information was used to switch the heater power as necessary to maintain operating temperature within the stack. The thermal controller was also wired to the serial output on the control panel for control by the LabVIEW user interface.

5.1.5.3 Pressure Transducer

The pressure transducer measured the pressure of the oxygen flow, which operated between 0 and 40 psig. The voltage output of the transducer was measured by one of the analog inputs of the data acquisition card. A pressure transducer was chosen over a mechanical gauge for space considerations, weight restrictions, and ease of measurement.

5.1.5.4 Oxygen Flow Meter

The flow meter recorded the rate at which oxygen is produced. The flow meter was also connected to one of the digital inputs on the data acquisition cards and was capable of measuring flow rates up to 5 sl/min.

5.1.5.5 Pressure Regulator

The pressure regulator on the control panel regulated the pressure of the oxygen outlet flow on the panel. This regulator worked in tandem with an internal pressure relief valve to assure that the system pressure did not cause the stack seals to separate and also maintained optimum production back pressure. The current design specified a back pressure of between 30 and 40 psi.

5.1.5.6 System Control Software

The entire system was controlled by a user interface built with the National Instruments LabVIEW programming language. The Graphical User Interface, which serves to access all system input and output information is shown in Figure 15. The user interface was implemented using a Pentium-equipped PC.

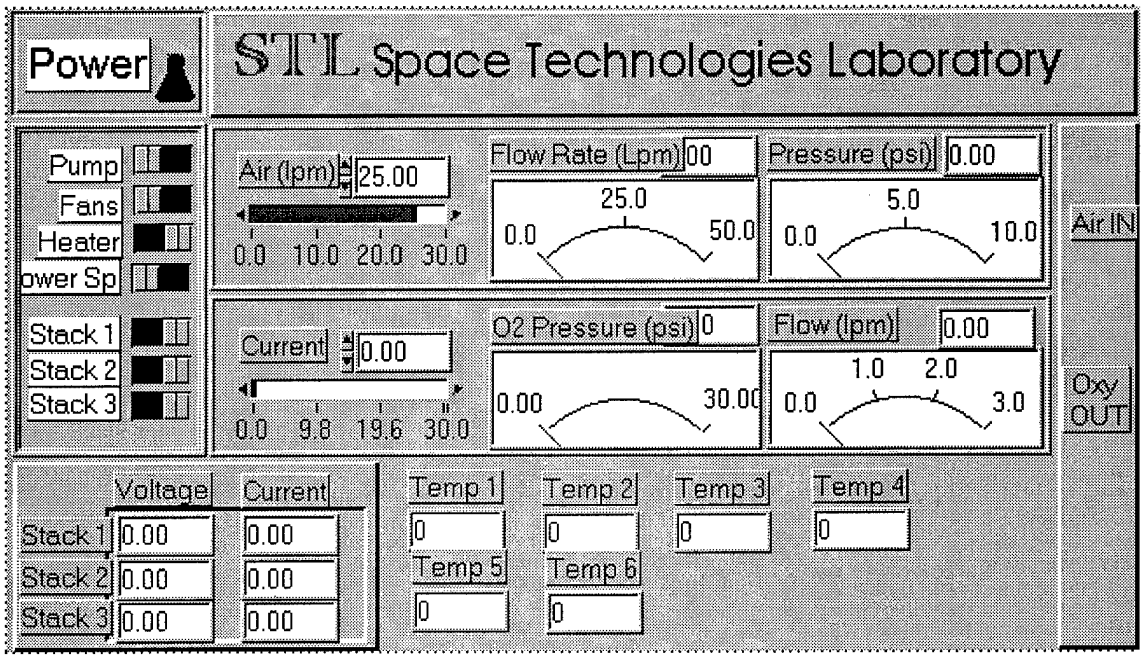

Figure 15. LabView interface.

5.1.6 Three to Five Cell Stack Assembly

A small stack testbed was designed to support the operation of a three to five cell stack. The test bed unit, (Figure 16) was to be used strictly as a desktop demonstration unit. While the configuration of all supporting structures was similar to the full stack design, the bracket assemblies pictured were built from readily available materials and constructed so as to provide maximum support for the small stack.

5.1.6.1 Stack Insulation

Since package size was not a concern, Btu-Block was the material chosen. The characteristics of this type of insulation are similar to the Min-k used in the full stack insulation except that thermal conductivity is slightly higher. Therefore higher temperatures

were experienced at the outer surfaces. The entire insulation assembly was enclosed in a tin container as seen in Figure 17, which served to protect the material from crumbling and losing its shape. Each surface of the stack and heater assembly was completely covered by this material as noted by the many layers.

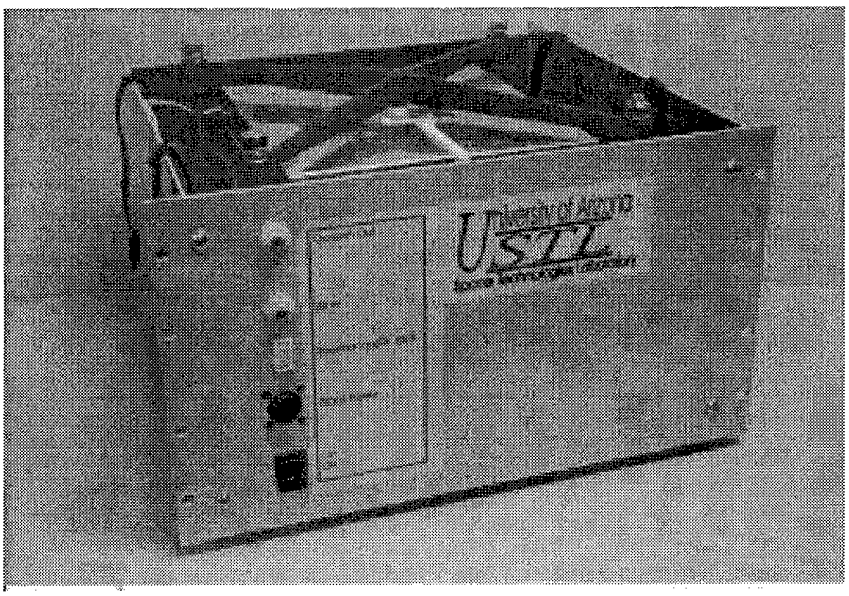

Figure 16. Small Stack Assembly

5.1.6.2 Stack Heaters

The heater elements were limited to a common 120 VAC single-phase wall outlet power source. The minimum rating of the heaters was 1000°C and, therefore, operating temperature was safely maintained. The elements themselves were located inside the insulation shown in Figure 17 and sit right next to the small stack during operation.

6. Cell Testing

6.1 Theoretical I-V Characteristics

The oxygen produced by each electrolyte plate is proportional to the current driving the stack. The current (I) needed to get a particular flow rate of oxygen (f in liters/min) is given by:

$$I = 78385.7\ (Pf\ /\ T\ \text{cell\#}) \qquad (4)$$

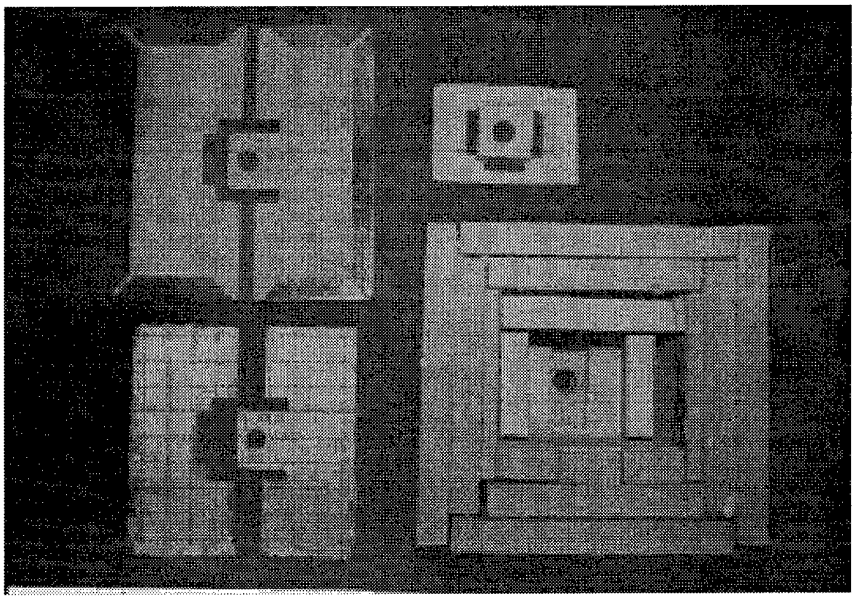

Figure 17. Stack housing and insulation.

where P is the pressure of the oxygen in atmospheres, T is the temperature, in Kelvin, and cell# is the number of cells in the stack. Since the cells are stacked in series the current through each cell will be the same.

The voltage needed to drive the generator at a given current is the result of the potential caused by the oxygen gradient across the electrolyte, the electrical resistance of the cell components and the polarization of the electrodes due to electrochemical resistance. The potential on each cell will be equal to the sum of these voltages and the voltage of the stack will be the sum of the voltages of each cell. The voltage of a stack (V) in volts is given by:

$$V = I/A\ [\ (\sigma_{electrolyte} \cdot t) + (\sigma_{separator} \cdot t) + \eta] + Er \qquad (5)$$

where A is the active area in cm^3, σ is resistivity in $\Omega \cdot cm^2$, t is the thickness of the component in cm, η is the area specific polarization resistance in $\Omega \cdot cm^2$, and Er is the potential produced from having a Po_2 gradient across the cell (Nernst potential). A theoretical base line of the cells expected performance was calculated using Eqns. (4) and (5).

6.2 Procedure

The testing of the cells was done using a four point method. Four platinum leads were used, two supply the current, to drive the cell, and two measure the voltage. One current and voltage contact was made through the manifold to the bottom gold seal while the other (current and voltage contact) made contact through an addition hole drilled in the manifold. Gas connections were made, and air was pumped through the stacks at rates greater than 400 sccm. The flow rates were controlled using a mass flow controller. The stack was placed in a Kanthal wound furnace and heated to the operating temperature (1000°C). The performance of the stacks was evaluated as a function of both current, temperature, and time. Tests were conducted on both a single cell and on three cell stack. The same testing procedure was used for both.

6.3 Single Cell Tests

An external view of the single cell stack is shown in Figure 18. The stack, including manifolding and external tubing, fits in the palm of a hand. A higher magnification of the stack (Figure 19) shows the seals, separator plates and electrolyte. The I-V curve for a single cell stack at several different operating temperatures is shown in Figure 20. Unfortunately, the stack did not seal completely and the cell voltage was slightly lower than expected. It should be noted that for this stack the initial voltage was quite high ($\approx$ 10 volts/cell) until the current reached 5-10 amps. It then dropped down too near the expected values. This was due to the high contact resistance between the cell components initially since there is only physical contact at the component surfaces. After the current reaches a high enough value to cause these high resistive contacts sinter together and the resistance decreases. This step of applying both high voltage and current to the stack is call conditioning and was carried out on all stacks assembled and tested. After the contact resistance decreased the measured I-V behavior was linear. The slope of the voltage versus current density curve gives the area specific resistance (ASR) of the cell. The ASR of the single cell shown in Figure 19 was 0.38 $\Omega \cdot cm^2$. This is equivalent to ASR's observed for stabilized zirconia tested as solid oxide fuel cells.

6.4 Stack Tests (3-cell Stack)

The performance of the three cell stack was evaluated as a function of time, temperature and current. The plot in Figure 21 shows the I-V behavior of the three cell stack at three operating temperatures in addition to the predicted I-V behavior. The ASR for the stack at 1000 °C was 1.25 $\Omega \cdot cm^2$ (0.41 $\Omega \cdot cm^2$ /cell) which is very near the predicted value of 1.20

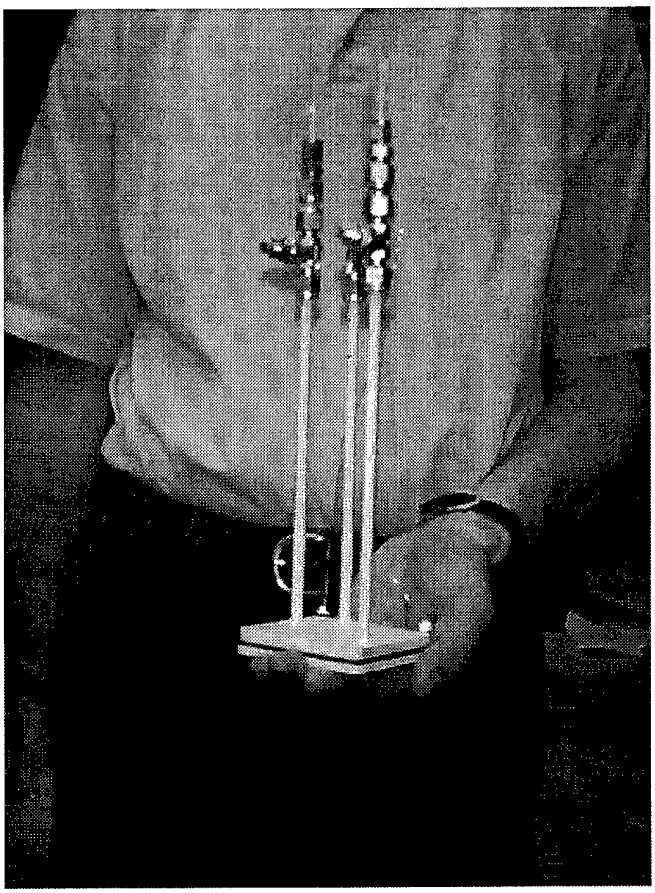

Figure 18. Single cell stack.

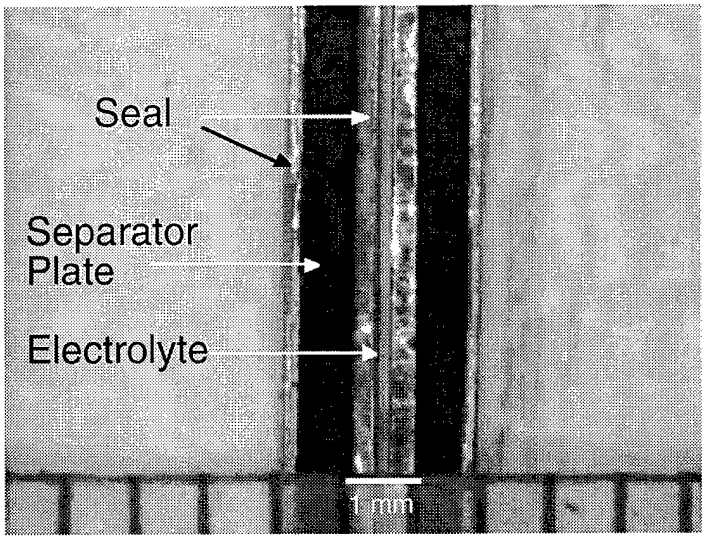

Figure 19. High magnification of manifolded single cell showing seals.

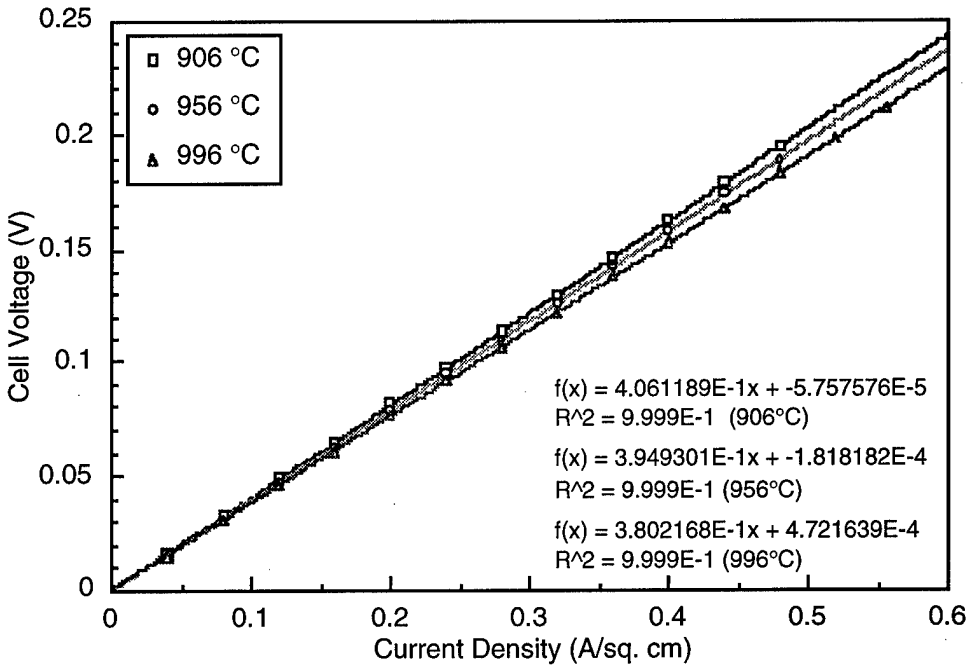

Figure 20. Current-voltage behavior of a single cell stack

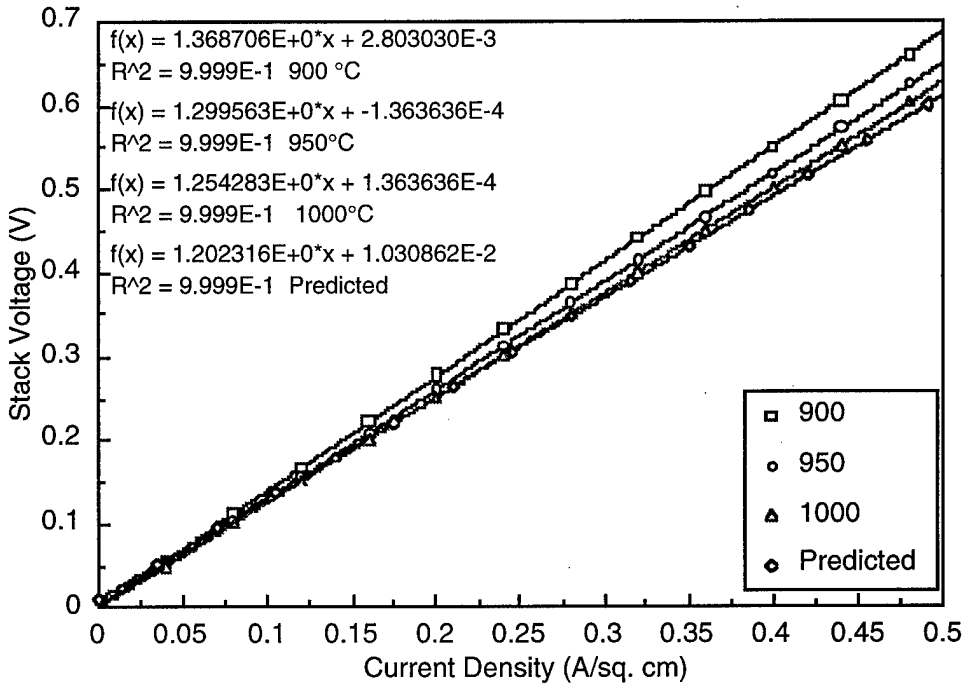

Figure 21. Current-voltage behavior of a single cell stack

$\Omega \cdot cm^2$ (0.40 $\Omega \cdot cm^2$ /cell). As with the single cell test the stack did not seal completely, therefore, the I-V curve deviates slightly from the predicted value.

The three cell stack performance was monitored as a function of time as shown in Figure 22. The stack was run at constant current while the voltage was measured as a function of time. The stack voltage decreased with time for both 4 and 7 amps. This decrease voltage is caused by a decrease in the stack resistance. This was confirmed by the ASR decreasing to the 1.05 $\Omega \cdot cm^2$ (0.35 $\Omega \cdot cm^2$/cell), after 4 days of operation as shown inFigure 23.

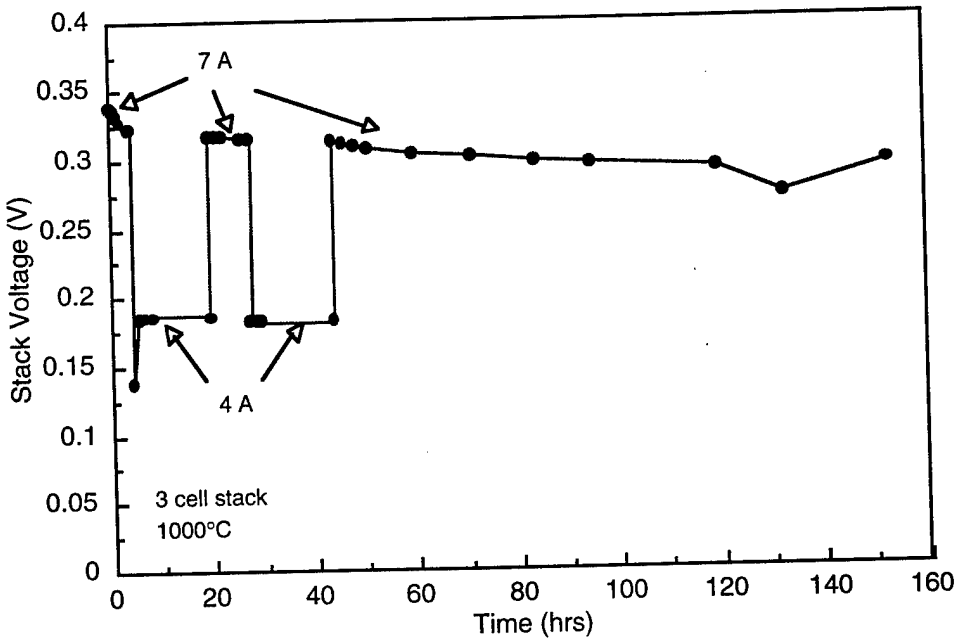

Figure 22. Stack performance with time under constant current conditions.

As with the single cell test the stack had to be conditioned with ≈ 10 volts/cell before operation could begin. This is an issue that will have to be addressed as the number of cells in each stack continues to increase. If, for example, a 70 cell stack were to be conditioned, it would require ≈700 volts which is excessively higher than the voltage needed to run the stack (< 30 volts). One possible solution would be to condition a smaller number of cells at a time (i.e. segment the stack in to bundles of 10 cells or less).

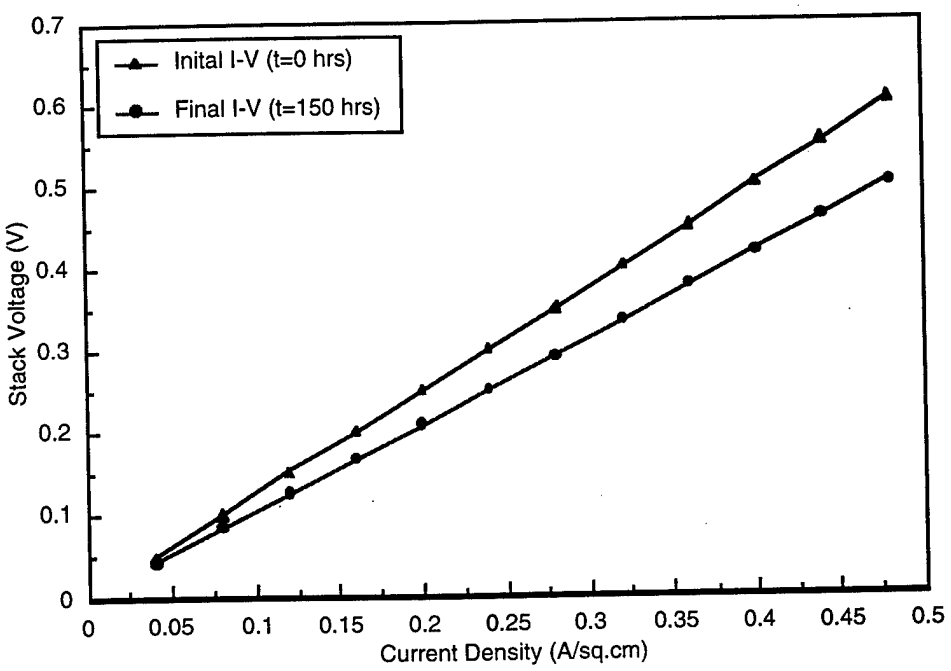

Figure 23. Voltage versus current density data of the 3-cell stack at t=o hrs and after t=150 hrs, showing decrease in ASR and improvement in stack performance.

The charge balance for oxygen is 3.78 ml/A, this yields an oxygen production of 1.05 ml/ cm^2•min for each square centimeter of active electrolyte area using the measured current density of 0.28 A/cm^2. In the 3-cell stack the total active electrolyte area was ≈75 cm^2, therefore, the total oxygen output can be calculated to be 79.3 ml/min (Figure 24).

The initial power consumption of the stack to produce 79 cc/min was 2.4 W. The power consumption to produce the equivalent amount of oxygen after 150 hours of stack operation was 2.0 W, a decrease of 18%. This was due to an improvement in the contact resistance with time. The oxygen separation efficiency for this stack was calculated to be ≈50%.

Post-mortum analysis on this outside stack indicated that there were no flaws or failures of the seal due to thermal expansion mismatches between the base materials and seal. Further studies have been carried out in which this stack was reheated to 1000°C and current was applied. Upon application of the current, the stack started to pump oxygen from air and had a current density of 0.28 A/cm^2 (7 A) and a potential of 0.29 V. This stack has now successfully thermal cycled 6 times, each time cycling between room temperature and 1000°C.

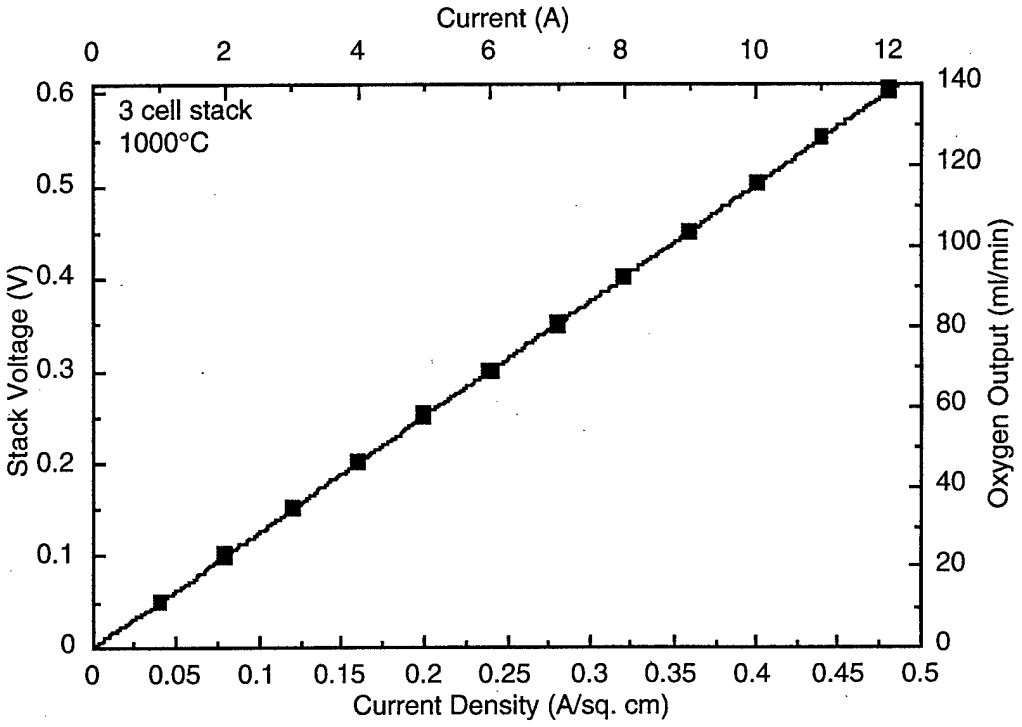

Figure 24. Stack voltage and oxygen output as a function of current density.

6.5 Discussion

The ultimate goal of for the U.S. Army is to develop a compact lightweight device that can deliver 3 l/min of pressurized oxygen. Using the data collected during this study is was estimated that a total active area of ≈1600 cm^2 would be required to produce that quantity of oxygen (assuming a current density of 0.5 A/cm^2). Assuming an active area of 25 cm^2, the stack would require 64 cells to produce 3 l/min. The size and mass of this stack would be approximately 125 in^3 (0.07 ft^3) and 2.2 lbs, respectively.

By extrapolating the data gained from testing the 3-cell stack, approximations can be made about the power consumption and performance of the 70-cell stack (1000°C operating temperature, 25 cm^2 active area). For example, to produce 1 liter/minute of oxygen under ambient conditions would require ≈15 W of power to drive the ceramic stack (Table 8). The final prototype device required by the U. S. Army must produce 3 liters of oxygen per minute at 40 psi (≈2.8 atm). Using the measured potential from the 3-cell stack (0.29 V at 7 A), the stack would require ≈144 W of power to produce the required oxygen. The amount of power can be reduced by either increasing the active area or increasing the number of cells in the stack. For example, an increase in the cell active area or in the number of cells in the stack by a factor of 2, decreases the power requirement by half (i.e.

70 cells with an active area of 100 cm^2 or 140 cells with an active area of 50 cm^2 would require ≈36W)

Table 8. Stack (70 cells) power needed to separate oxygen from air at 1000°C using a stabilized zirconia electrolyte with a 25 cm^2 active area.

Pressure (atm)	Flow Rate (liters/minute)		
	1	2	3
1	15.0	16.4	17.0
2	63.4	65.7	67
3	138	142	144

7. Conclusions

This project demonstrated that within one year a small scale prototypical oxygen generator could be constructed and successfully tested at 1000°C. The stack tests indicated that: 1) all 25 cm^2 of the active area was operational, 2) the cells possessed a low ASR that improved with time, 3) stack power consumption decreased with time without affecting oxygen output, and 4) none of the operational stacks failed during this program. Important accomplishments were achieved in the areas of separator plate fabrication, metallic seal development, and stack assembly and sealing.

The technical accomplishments of this program were:

- A conceptual design for the oxygen generator was developed
- A reliable and scaleable fabrication method for the fabrication of complex shaped separator plates was developed.
- A metallic braze seal was developed and successfully tested to seal LSM separator plates to stabilized zirconia electrolytes.
- Numerous stacks were assembled to evaluate seals and for electrical testing
- A single cell and 3-cell stack were successfully tested.
- A small lightweight power suppliy was constructed to operate the oxygen generator.
- A lightweight furnace was constructed using Min-K insulation to contain the generator during operation.
- Stack performance met expectations with:
  - all 25 cm^2 of the active area was operational
  - a low ASR recorded for the cells

- stack power consumption decreasing with time without affecting oxygen output

8. References

1. Y. M. Tamura, M. Kawai, K. Nomura, Y, Nakamura, and O. Yamamoto, Solid Oxide Fuel Cells IV, M. Dokiya et al. (eds), Proc. Electrochem. Soc., 95 (1) 30 (1995).
2. T. Ishihara, H. Matsuda, and Y. Takita, J. Am. Ceram. Soc., **116** 3801 (1994).
3. M. Feng and J. B. Goodenough, J. Solid State Inorg. Chem., **31** 663 (1994).
4. A. Petric, P. Huang, and An. Skowron, Proc. of the Second European Solid Oxide Fuel Cell Forum, ed. by B. Thorstensen, p 751, Oslo, Norway, (1996).
5. Conceptual Design for a Ceramic Oxygen Generator CNT N62269-94-C-1284, Sponsor Naval Air Warfare Center, Aircraft Division, Warminster, PA.
6. N. Q. Minh, J. Am. Ceram. Soc., **76** 563-88 (1993).
7. N. Q. Minh and T. Takahashi, Science and Technology of Ceramic Fuel Cells, Elsevier, The Netherlands, (1995).
8. J. A. Mangels and G. L. Messing, Advances in Ceramics, Vol. 9: Forming of Ceramics, The American Ceramic Society, Columbus, Ohio, (1984).
9. G. Y. Onoda Jr. and L. L. Hench, Ceramic Processing Before Firing, John Wiley and Sons, Inc., New York, New York, (1978).

Appendix A.1

Summary of Glass Seal Condition and Quality.

Identification Number	Heating Rate (°C/min)	Soak Temp (°C)	Soak Time (min)	Cooling Rate (°C/min)	Observations
GS001	5	1000	180	5	Sintered, well bonded to substrate through melting of glassy phase. Not enough fluidity for a hermetic seal without high pressure assistance.
GS03	>200	1000	60	5	Similar to GS001
GS004	10	1350	180	5	Well bonded to substrate. Complete remelt of Material K. Excellent fluidity. Heavy crystallization (brown colored) when cooled to room temperature
GS005	>200	1350	45	~200	Well bonded to substrate. Complete remelt of Material K. Excellent fluidity. Light crystallization (brown colored) when cooled to room temperature
GS006	>200	1350	30	>200	Well bonded to substrate. Complete remelt of Material K. Excellent fluidity. Minimal crystallization (brown colored) when cooled to room temperature
GS008	10	1205	180	10	Well bonded to substrate through melting of glassy phase and partial crystalline phase dissolution. Marginal fluidity for a hermetic seal without pressure assistance. Heavy crystallization (brown colored) when cooled to room temperature
GS009 GS010	>200	1205	45	>200	Well bonded to substrate through melting of glassy phase and partial crystalline phase dissolution. Marginal fluidity for a hermetic seal without some pressure assistance. Minimal crystallization (brown colored) when cooled to room temperature

GS021	10	1255	180	10	Well bonded to substrate through melting of glassy phase and partial crystalline phase dissolution. Marginal fluidity for a hermetic seal without some pressure assistance. Heavy crystallization (brown colored, but smaller crystalline grains) when cooled to room temperature
GS022	10	1255	90	>200	Well bonded to substrate through melting of glassy phase and partial crystalline phase dissolution. Marginal fluidity for a hermetic seal without some pressure assistance. Less crystallization (brown colored, but smaller crystalline grains) when cooled to room temperature
GS023	>200	1255	90	10	Well bonded to substrate through melting of glassy phase and partial crystalline phase dissolution. Marginal fluidity for a hermetic seal without some pressure assistance. More crystallization (brown colored, but smaller crystalline grains) than GS022 when cooled to room temperature
GS015	10	1158	180	10	Well bonded to substrate through melting of glassy phase and partial crystalline phase dissolution. Marginal fluidity for a hermetic seal without some pressure assistance. Heavy crystallization (brown colored, but smaller crystalline grains) when cooled to room temperature
GS016 GS017	>200	1158	30	10	Sintered, well bonded to substrate through melting of glassy phase. Not enough fluidity for a hermetic seal without high pressure assistance.
GSS001 from GS027 GS028	>200	1255	50	>200	Well bonded to both substrate through melting of glassy phase and partial crystalline phase dissolution. Slight fluidity enhancement compared to GS021, GS022 and GS023, due probably increased material (twice as much since GSS001 is from two individual seal pieces.

Appendix A.2

Micrographs of Seal Tests

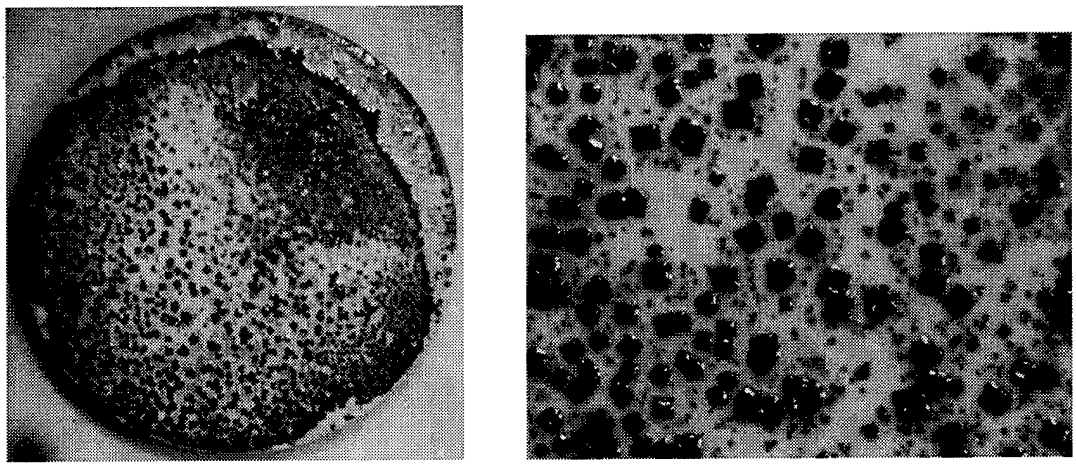

Figure 1. Optical micrograph of glass seal (GS004) and high magnification of crystallites in glass. Largest crystallites are ≈100 μm.

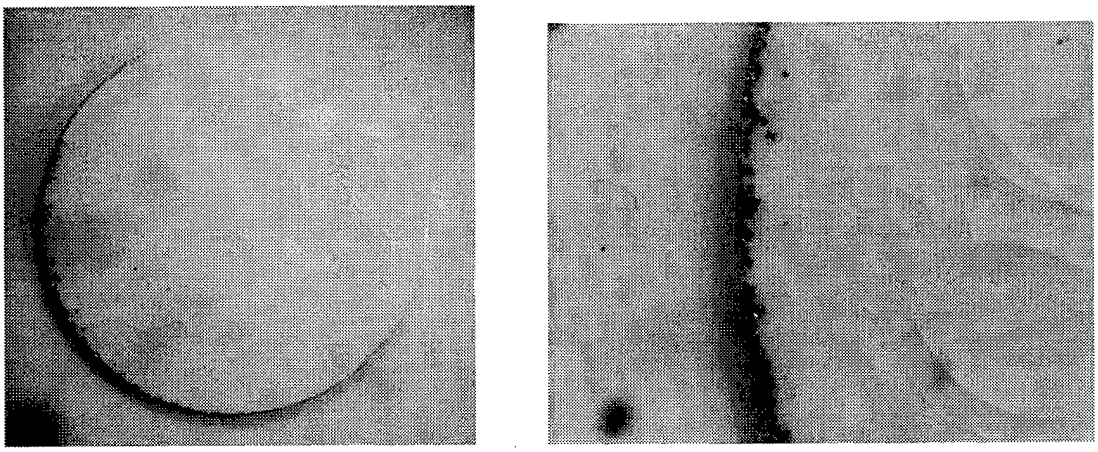

Figure 2. Optical micrograph of glass seal (GS006) and high magnification of glass showing cracking in glass matrix.

Bibliography

List of personnel receiving pay from this effort

B. L. Armstrong
T. R. Armstrong
R. J. Barbera
S. D. Burton
G. Coffey
D. A. Conner
W. J. Crayne
G. R. Golcar
M. Gong
R. M. Gore
D. B. Mackey
Y. Peng
L. R. Pederosn
M. J. Schweiger
K. L. Simmons
S. O. Slate
D. E. Smith
P. A. Smith
L. Thomas
L. J. Woodcock